Simultaneous Estimation of Wheel-Rail Adhesion and Brake Friction Behaviour ⋆

Christoph Schwarz * **Alexander Keck** *

* *German Aerospace Center (DLR), Institute of System Dynamics and Control, 82234 Wessling, Germany (e-mail: [christoph.schwarz, alexander.keck]@dlr.de).*

Abstract: In the field of longitudinal train dynamics the brake process is not only a safety critical aspect but it also determines the capacity of the rail network. Therefore, a reduction of the brake distance increases the safety level and the network capacity at the same time. However, to implement an advanced brake control set-up, the knowledge of the wheel-rail adhesion and the brake pad-disc friction is usually necessary. Since the direct measurement of these determining parameters is not reasonable due to technical and economic reasons, the present work presents an estimator framework for their online identification. To ensure a robust and reliable performance of the estimator, a generic wagon model is designed and the observability of the nonlinear system is evaluated. Furthermore, a reasonable synthesis of an extended Kalman filter is discussed that takes account of the system characteristics. In the end, the test results from a roller rig verify the accurate and robust performance of the developed estimator and confirm the great potential of such a concept in the context of mechatronic railway systems.

Keywords: Rail traffic, nonlinear systems, friction estimation, extended Kalman filter.

1. INTRODUCTION

Railway vehicles offer some essential benefits in comparison to other transportation systems such as motorized individual transportation. From a societal point of view the currently most relevant benefits are the higher capacity in urban traffic and the better ecological balance, see Umweltbundesamt (2019). However, in the long-distance sector the rail traffic capacity is limited by stringent restrictions related to the distance between trains. To overcome this limitation, the European Train Control System (ETCS), which slowly but surely finds its way into the railway network, allows for an operation with absolute braking distance. To fully exploit the potential of this concept and further increase the capacity of the existing railway infrastructure, the minimum distance between trains might be reduced by an optimized brake control.

In contrast to existing brake control systems, like wheel-slide protection (WSP) and load-dependent brake systems, an advanced control set-up requires additional information on the varying system properties. As shown in Schwarz et al. (2019a) the two most relevant parameters that have to be identified during the braking process are the wheel-rail adhesion and the friction coefficient in the brake pad and disc interface. Since there is no direct way to measure either of these parameters, in Ricciardi et al. (2017) a method is described to identify the brake unit friction via an estimator. Also for the wheel-rail adhesion estimation a row of elaborate concepts are proposed, like Charles et al. (2008); Shrestha et al. (2019); Strano and Terzo (2018); Ward et al. (2012). Based on these works the authors developed a wheel-rail adhesion estimation concept for a running gear with independently rotating wheels in Schwarz and Keck (2019). The approaches presented in Schwarz et al. (2019a,b) show first promising results of the simultaneous friction and adhesion estimation in a test rig environment and for track tests. Nevertheless, the combined, simultaneous estimation of both phenomena is not yet fully investigated, since in Schwarz and Keck (2019) the brake friction is not considered and in Schwarz et al. (2019a,b) only good adhesion conditions are tested. Therefore, the following work presents how to improve the robustness, reliability, and accuracy of an adhesion and friction estimator in the face of challenging scenarios like wheel-slide protection and sanding, what is necessary for a safe operation in the rough railway environment.

First of all, a generic model of the longitudinal dynamics of a railway vehicle is illustrated in section 2. Furthermore, the observability of the nonlinear system is analyzed, to verify the reliable functionality of the estimator in the entire operating range. In section 3 the applied observer concept and the test rig environment are described. Afterwards section 4 presents and discusses the estimation results of the challenging test scenarios. In the end, section 5 draws a conclusion, highlights the contributions to the field of mechatronic railway systems, and names the upcoming tasks that have to be tackled.

2. MODELING AND OBSERVABILITY ANALYSIS OF LONGITUDINAL RAILWAY DYNAMICS

The focus of the presented investigation on the longitudinal dynamics allows us to neglect the lateral dynamics.

⋆ This work was partially funded by StMWi (StMWi Grant Number: MST-1308-0006//BAY 191/002), the Bavarian Ministry of Economic Affairs and Media, Energy and Technology, within the project DynORail.

This substantially reduces the computational effort of the estimator algorithm and makes the transfer to a control unit a lot easier. According to this 2-D system consideration in the $x-z$ plane the longitudinal and vertical wheel-rail forces of the left and right wheel of one wheelset are merged into one F_x and one F_z, respectively. The same holds for the multiple brake units of one wheelset, so that Fig. 1 shows the scheme of a wagon as it is used in this work. The subscripts f and r represent the front and rear part of the wagon, i.e. $F_{x,i}$ using the index i=f, r denotes the longitudinal wheel-rail force at the front and rear wheelset, respectively. Analogously the vertical wheel-rail force is $F_{z,i}$. The other variables and parameters are described in the following paragraph. Considering only one wagon seems appropriate, since this enables a distributed estimator design for each specific wagon. This offers an advantage especially in case of an electric multiple unit, where the adhesion behavior varies between the heavy motor and light trailer cars.

To set up the nonlinear formulation of the system, the first step is to define the longitudinal force equilibrium

$$m \cdot \dot{v}_x = F_{\mathrm{TR}} + k_{\mathrm{d}} \cdot v_x^2 + F_{x,\mathrm{f}} + F_{x,\mathrm{r}}, \tag{1}$$

with the wagon mass m, the translational velocity v_x, the track resistance force F_{TR}, see Schindler (2014), and the drag factor k_{d} that includes the drag coefficient, drag area, and mass density of air. The longitudinal creep forces are influenced by the wheel-rail adhesion coefficient μ_{W}

$$F_{x,i} = \mu_{\mathrm{W}} \cdot F_{z,i}. \tag{2}$$

Only one μ_{W} is stated for the wagon, since it is assumed that the adhesion conditions do not significantly vary between the two wheelsets. The dynamic behavior of μ_{W} could be implemented according to well-established theories like Polach (2005). However, the parametrization of these models fits only for one specific condition, e.g. wet or dry. In order to prevent the observer prediction model from being wrongly parametrized, μ_{W} is implemented as

$$\dot{\mu}_{\mathrm{W}} = 0, \tag{3}$$

so that the time varying behavior of the adhesion coefficient is not regarded in the estimator prediction step but solely in the correction step. The wheelset load $F_{z,i}$ and its variation, respectively, depend on the construction and positioning of the traction rod. In the following a generic relation between $F_{z,i}$ and the longitudinal acceleration $\dot{v}_x$ is chosen

$$F_{z,i} = \frac{m}{2} \cdot g \pm \frac{h}{a} \cdot m \cdot \dot{v}_x, \tag{4}$$

with gravity constant g, height of the wagon's center of mass h and longitudinal wheelset distance a. Combining (1)-(4) leads to

$$\dot{v}_x = \frac{1}{m}\left(F_{\mathrm{TR}} + k_{\mathrm{d}} \cdot v_x^2\right) + \mu_{\mathrm{W}} \cdot \frac{g}{2}. \tag{5}$$

After the definition of the longitudinal force equilibrium the moment equilibria of the wheelsets around their lateral axes are considered

$$J_y \cdot \dot{\omega}_i = F_{\mathrm{B},i} \cdot r_{\mathrm{B}} + F_{x,i} \cdot r_{\mathrm{W}} + M_{\mathrm{W},i}. \tag{6}$$

The parameters in (6) are the wheelset inertia J_y, the brake radius r_{B}, and the wheel radius r_{W}. The dynamic variables are the angular wheelset velocity ω_i, the brake force $F_{\mathrm{B},i}$, and the additional wheel torque $M_{\mathrm{W},i}$, which includes for example the motor torque as well as the bearing/rolling resistance, see Schindler (2014). Analog to (2) the brake force

$$F_{\mathrm{B},i} = \mu_{\mathrm{B},i} \cdot F_{\perp,i} \tag{7}$$

depends on the friction coefficient in the brake unit interface $\mu_{\mathrm{B},i}$ and the pressing force of the brake pad $F_{\perp,i}$. The implementation of the brake friction dynamics can be done in the same way as it is described for the wheel-rail adhesion, i.e.

$$\dot{\mu}_{\mathrm{B},i} = 0. \tag{8}$$

Another reasonable formulation of the brake friction dynamics is a first order characteristic

$$\dot{\mu}_{\mathrm{B},i} = \frac{\mu_{\mathrm{B},0} - \mu_{\mathrm{B},i}}{t_\mu \cdot \mu_{\mathrm{B},i}}, \tag{9}$$

with the initial estimation of the brake friction coefficient $\mu_{\mathrm{B},0}$ and the time constant t_μ. This implementation of $\dot{\mu}_{\mathrm{B},i}$ is a significantly simplified version of the approach presented in Ostermeyer (2003). The decision whether to use (8) or (9) is a trade-off between an easier implementation in (8) (since there are no additional parameters to be defined) and a slightly more accurate modeling in (9). As mentioned at the beginning of this section it is tried to keep the system as simple as possible for the sake of real-time capability so that the variant in (8) is used. The angular acceleration is

$$\dot{\omega}_i = \frac{1}{J_y}\left(\mu_{\mathrm{B},i} \cdot F_{\perp,i} \cdot r_{\mathrm{B}} + \mu_{\mathrm{W}} \cdot f_{\mathrm{sub}} \cdot r_{\mathrm{W}} + M_{\mathrm{W},i}\right), \tag{10}$$

with the substitution

$$f_{\mathrm{sub}} = \frac{m}{2} \cdot g\left(1 \pm 2 \cdot \frac{h}{a} \cdot \mu_{\mathrm{W}}\right) \pm \frac{h}{a}\left(F_{\mathrm{TR}} + k_{\mathrm{d}} \cdot v_x^2\right). \tag{11}$$

Assuming that usually $2 \cdot \frac{h}{a} \cdot \mu_{\mathrm{W}} \ll 1$ the nonlinear system with an additional linear input $\boldsymbol{u}_{\mathrm{lin}}$ reads

$$\begin{aligned}
\dot{\boldsymbol{x}} &= \boldsymbol{f}(\boldsymbol{x},\boldsymbol{u}) + \boldsymbol{B}\boldsymbol{u}_{\mathrm{lin}} = \\
&= \begin{pmatrix}
\frac{1}{J_y}\left(r_{\mathrm{B}} x_4 u_1 + r_{\mathrm{W}} x_6 \left(\frac{mg}{2} + \frac{h\left(u_3 + k_{\mathrm{d}} x_3^2\right)}{a}\right)\right) \\
\frac{1}{J_y}\left(r_{\mathrm{B}} x_5 u_2 + r_{\mathrm{W}} x_6 \left(\frac{mg}{2} - \frac{h\left(u_3 + k_{\mathrm{d}} x_3^2\right)}{a}\right)\right) \\
\frac{1}{m}\left(\frac{mg}{2} x_6 + u_3 + k_{\mathrm{d}} x_3^2\right) \\
0 \\ 0 \\ 0
\end{pmatrix} \\
&\quad + \begin{bmatrix}
\frac{1}{J_y} & 0 & 0 & 0 & 0 & 0 \\
0 & \frac{1}{J_y} & 0 & 0 & 0 & 0
\end{bmatrix}^T \boldsymbol{u}_{\mathrm{lin}},
\end{aligned} \tag{12}$$

with the state vector

$$\boldsymbol{x} = [\omega_{\mathrm{f}}, \omega_{\mathrm{r}}, v_x, \mu_{\mathrm{B,f}}, \mu_{\mathrm{B,r}}, \mu_{\mathrm{W}}]^T \tag{13}$$

and the nonlinear and linear input vectors

$$\boldsymbol{u} = [F_{\perp,\mathrm{f}}, F_{\perp,\mathrm{r}}, F_{\mathrm{TR}}]^T, \quad \boldsymbol{u}_{\mathrm{lin}} = [M_{\mathrm{W,f}}, M_{\mathrm{W,r}}]^T. \tag{14}$$

The measurement signals are the longitudinal wagon velocity and the angular wheelset velocities, so that the linear output equation is

$$\boldsymbol{y} = \boldsymbol{C}\boldsymbol{x} = \begin{bmatrix} 1&0&0&0&0&0 \\ 0&1&0&0&0&0 \\ 0&0&1&0&0&0 \end{bmatrix} \boldsymbol{x}. \tag{15}$$

After the description of the system design the observability has to be evaluated, to ensure the reliable performance

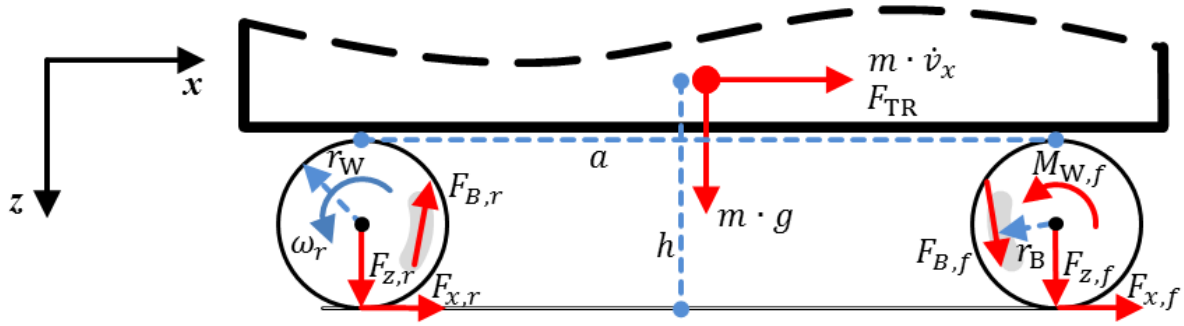

Fig. 1. Forces, torques and kinematics of a generic wagon

of the estimator framework. Equation (12) reveals the nonlinearities of the system, which demand for a nonlinear observability analysis according to Gauthier et al. (1992); Hermann and Krener (1977). There it is stated that a nonlinear system is observable, if $\boldsymbol{h}^{-1}(\boldsymbol{z})$ exists, with

$$\boldsymbol{z} = \boldsymbol{h}(\boldsymbol{x}) = \left[\boldsymbol{y}, \dot{\boldsymbol{y}}, \cdots, \boldsymbol{y}^{(n-1)}\right]^T. \tag{16}$$

The parameter n denotes the system dimension, which is in our case $n = 6$. To verify the observability, it is often not necessary to calculate the $(n-1)$th derivation of $\boldsymbol{y}$. For the system (12) and (15) the first derivation already allows for the formulation of $\boldsymbol{h}^{-1}(\boldsymbol{z})$. Neglecting the linear input, the inversion of $\boldsymbol{h}(\boldsymbol{z})$ is

$$\boldsymbol{x} = \begin{pmatrix} z_1 \\ z_2 \\ z_3 \\ \dfrac{J_y z_4 - r_W f_{\text{sub,z}} \left(1 + \frac{2h\left(u_3 + k_d z_3^2\right)}{amg}\right)}{r_B u_1} \\ \dfrac{J_y z_5 - r_W f_{\text{sub,z}} \left(1 - \frac{2h\left(u_3 + k_d z_3^2\right)}{amg}\right)}{r_B u_2} \\ \dfrac{2}{mg} f_{\text{sub,z}} \end{pmatrix}, \tag{17}$$

with the substitution

$$f_{\text{sub,z}} = m z_6 - u_3 - k_d z_3^2. \tag{18}$$

Lines four and five of (17) reveal that the system is not observable, when $u_1 = 0$ and $u_2 = 0$. This aspect has to be taken into account especially in case of a braking scenario with wheel-slide protection, where the pressing force is abruptly reduced and the contact between pad and disc is lost. An estimator set-up that shows a reliable performance in this critical state is described in the following section.

3. TEST FRAMEWORK AND ESTIMATOR SET-UP

In order to find a robust estimator parametrization and to verify the reliable and accurate performance of the estimator, a test rig environment offers some deciding benefits in contrast to track tests. First of all, challenging environmental conditions, like a wet and slippery interface between wheel and rail, can be regulated via the controlled injection of water and oil, respectively. The second benefit is the extended set of measurement equipment that allows for a quantitative evaluation and validation of the wheel-rail adhesion. The authors are aware of the fact that the reduction to a single wheelset prevents a general verification of the estimator performance with respect to an entire train. Nevertheless, a performance test within this reduced and reproducible test rig environment seems to be a reasonable first step before executing track tests that require an extensive technical and economic effort. Thus, the roller rig illustrated in Fig. 2 and described in Schwarz et al. (2019a) is used for the estimator tests. On this test rig only a single wheelset is operated and therefore the system in (12) has to be reduced by the second wheelset. The resulting state vector is

$$\boldsymbol{x} = \left[\omega_W, v_x, \mu_B, \mu_W\right]^T, \tag{19}$$

with the angular wheelset velocity ω_W and the virtual longitudinal velocity $v_x = \omega_{\text{Roller}} r_{\text{Roller}}$. Amongst other signals the longitudinal and vertical wheel-rail contact forces are measured via load cells mounted in the longitudinal and vertical cylinders, highlighted in orange in Fig. 2. Thus, according to (2) the actual adhesion coefficient is the quotient of the measured longitudinal and vertical wheel-rail force. Furthermore, additional torques can be applied directly to the roller and the wheelset, to reproduce inertia and other resistance effects. In the presented configuration only the roller is affected by an additional torque that imitates drag resistance and the longitudinal inertia of a wagon.

As described in the previous section the system is nonlinear, so that a nonlinear estimator has to be used. A well-established method that proves its worth for a railway application in Schwarz et al. (2019b) is the extended Kalman filter (EKF). For a detailed discussion of the

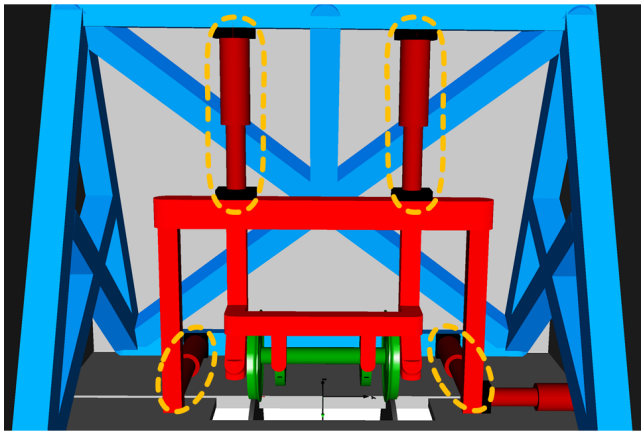

Fig. 2. Digital twin of the roller rig at Knorr-Bremse in Munich

EKF see Simon (2006) and Brembeck et al. (2014). The estimator behavior can be influenced via two covariance matrices, which are usually defined as diagonal matrices. The first one is the system noise covariance matrix $\boldsymbol{Q}$, which describes how much the estimator relies on the prediction model (12). The second covariance matrix $\boldsymbol{R}$ refers to the measurement noise, i.e. low diagonal entries R_{ll} correspond to a high trust in the measurement signals $\boldsymbol{y}$. According to the number of system states and outputs at the test rig there are four system noise parameters Q_{jj} and two measurement noise parameters R_{ll}.

Typical values for Q_{jj} and R_{ll} range from 10^{-9} (high trust in the system state or measurement signal) to 10^{1} in case of a very low trust in the respective state or measurement signal. Thus, to achieve a good estimator performance, the tuning of the covariance matrices has to consider the system design and the physical characteristics of the states. Determining the estimator parameters via a numerical optimization as done in Schwarz and Keck (2019) would involve two significant concerns. Firstly, the optimization result highly depends on the objective function and in the present case it is anything but trivial to identify a reasonable objective function, since three aspects have to be simultaneously considered: adhesion, brake friction, and kinematics, i.e. wheel and roller velocities. Secondly, the nonlinearity of the brake friction, which is not taken into account in Schwarz and Keck (2019), usually leads to several solutions of the optimization problem and, thus, the found optimum might be a local optimum. Therefore, in the present work the noise covariance matrices are manually defined in accordance with physical and technical system properties

$$\boldsymbol{Q} = \begin{bmatrix} 10^{1} & 0 & 0 & 0 \\ 0 & 10^{-5} & 0 & 0 \\ 0 & 0 & 10^{-3} & 0 \\ 0 & 0 & 0 & 10^{-1} \end{bmatrix}, \; \boldsymbol{R} = \begin{bmatrix} 10^{-9} & 0 \\ 0 & 10^{-7} \end{bmatrix}. \quad (20)$$

The parameter Q_{44} referring to the wheel-rail adhesion is set to a high value, since the generic definition of $\dot{\mu}_{\mathrm{W}}$ in (3) does not describe the actual adhesion behavior in an overbraking scenario when the adhesion abruptly changes. In contrast, the dynamic behavior of the brake friction coefficient μ_{B} is comparably slow, so that the trust in (8) is higher than in (3) and Q_{33} has got a value of 10^{-3}. The two parameters R_{22} and Q_{22} related to v_x are set in a medium range with 10^{-7} and 10^{-5}, respectively. This means the modeling comprises most of the influences but not all of them like for example wind, which cannot be reasonably integrated in the dynamic model. Regarding the parameters related to ω_{W} the trust in the measurements is rated higher than the trust in the model, i.e. $R_{11} = 10^{-9} < Q_{11} = 10^{1}$, due to the simplifications made in the system design. The definition of the parameter values at the upper and lower end of the range turns out to be necessary to achieve reliable adhesion results, what can be explained with the help of Fig. 3. The critical situation for the estimator arises in point 2, when the wheel-slide protection (WSP) becomes active. In a real railway system two relevant aspects can be observed after that point: the wheelset accelerates, i.e. $\dot{\omega} > 0$, and μ_{W} goes the same way back to point 1 that it took from point 1 to point 2 before the WSP activation. If R_{11} is too high or Q_{11} is too low, the estimator suggests that

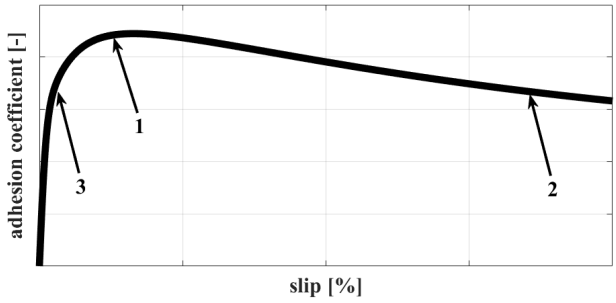

Fig. 3. Qualitative scheme of a typical adhesion over slip characteristic

an increasing wheelset velocity is induced by a decreasing adhesion just as it is the case when we go from point 1 to point 3. To prevent this misleading estimation result, R_{11} has to be set to a very low value although this sacrifices the noise reducing property of the Kalman filter. After the description and discussion of the estimator set-up the following section highlights some results of the test rig experiments.

4. RESULTS OF THE ESTIMATOR TESTS

For the estimator analysis at the test rig two different test types are executed. In one case an almost continuous WSP is provoked and in the other case sanding is activated. With these challenging scenarios the robustness and reliability of the estimator in rough operating conditions can be validated. In the following, one representative scenario of each test type is presented. The velocity and pressing force profiles of the WSP test are illustrated in the upper part of Fig. 4. In the beginning between 18s and 33s there are three distinct, short-time brake applications and at about 42s the stop brake application is induced. The low pressing force in combination with the high slip indicates a low adhesion level, what is confirmed by the lower diagram. In this lower diagram the measured and estimated adhesion is shown together with the estimated brake friction. Both adhesion profiles almost identically depict the three brakings at the beginning and the low adhesion phase between 42s and 110s with values of only 0.02-0.05. The high-frequency oscillations from about 110s until the end are good approximated as well. The only deviation occurs in the first few tenths of a second, when the initialization errors of the estimator are corrected. The friction profile illustrated by the solid red line shows the typical increasing behavior from 110s on that correlates with the decreasing wheelset velocity. Since it is not possible to measure the actual value of μ_{B} at the test rig, the friction results could only be qualitatively verified by brake experts on an experience base. Thus, one of the remaining tasks is to confirm the friction estimation in dynamometer tests. We skip the estimations of ω_{W} and v_x, since there is no remarkable difference between the measured and estimated data, what is expected due to the use as estimator inputs.

The input and measurement data for the estimator in the sanding scenario are shown in the upper plot of Fig. 5. The initial velocity is with 200km/h higher than in the first scenario with 120km/h. Furthermore, the WSP application is reduced in contrast to the first scenario what

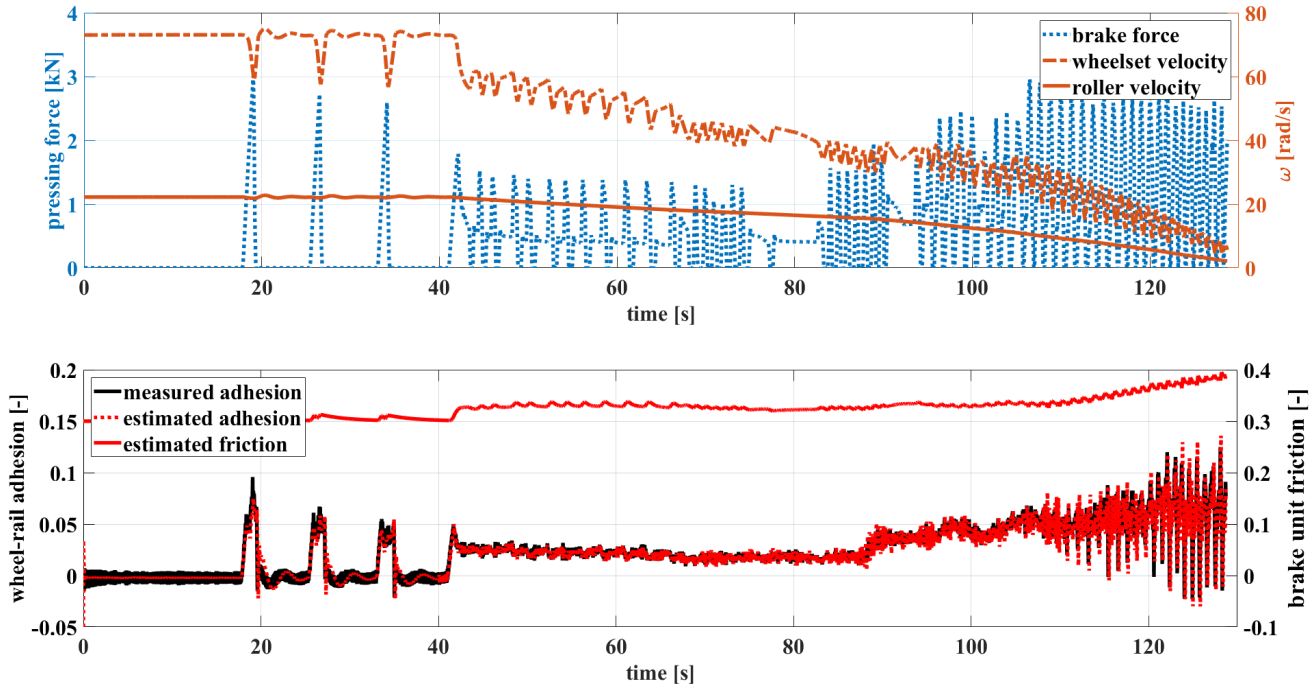

Fig. 4. Top: System input and measurement data provided to the observer; bottom: Estimation results together with measured adhesion in the wheel-slide protection scenario

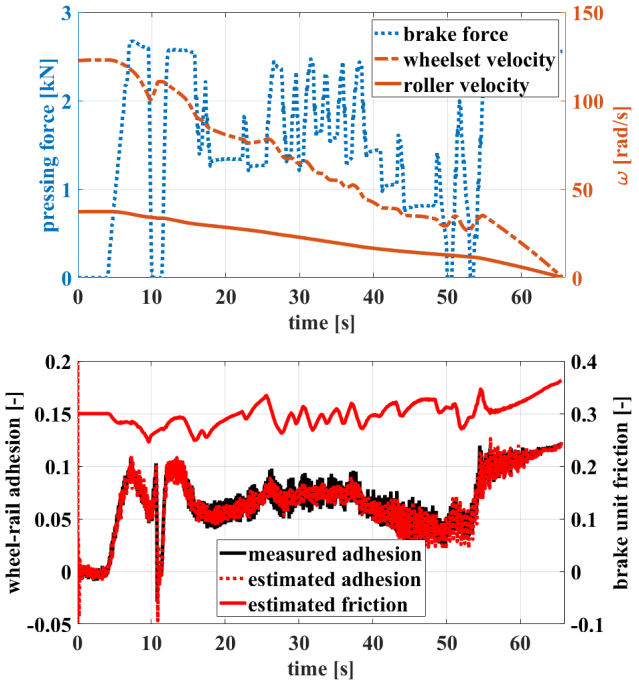

Fig. 5. Top: System input and measurement data provided to the observer; bottom: Estimation results together with measured adhesion in the sanding scenario

results in a lower frequency of the pressing force changes. This difference is founded in the sanding application what leads to an increased adhesion level, see the lower part of Fig. 5. Before discussing the adhesion results the focus is on the brake friction estimation. The larger oscillations of μ_B occur due to the aforementioned lower frequency of $F_\perp$. This means the slow dynamic of μ_B is in this scenario able to follow the different pressing force levels. This aspect and the increasing behavior of the brake friction from 55s until the end verify the plausibility of the friction estimation.

The wheel-rail adhesion shows at the beginning the same initialization behavior like in Fig. 4. However, the probably most relevant part is between 4s and 11s, when firstly the adhesion drops from its maximum at 0.1 to 0.05 and then the pressing force is released so that μ_W jumps back to 0.1 before it falls down to 0. This is exactly the critical behavior discussed in the previous section along with Fig. 3. Analog to Fig. 3 the estimated and measured adhesion results are illustrated in Fig. 6 in an adhesion-over-slip diagram. It can be seen that over the entire slip range the correlation between the two adhesion profiles is high and the decreasing behavior of the adhesion coefficient is well imitated. The lower plot shows the estimation error between measured and estimated adhesion coefficients and confirms the good performance of the estimator for each slip level. The only peak higher than 0.02 occurs during wheel-slide protection. This deviation is identified by the observer within 0.1s, what is faster than the usual wheel-slide protection control with a response time of about 0.2s. In the end, the robustness and reliability of the presented estimator set-up are verified by two different test cases and in both of them the results of the adhesion estimation are highly accurate.

5. CONCLUSIONS AND OUTLOOK

The previous sections describe in detail the design process of an estimator for the adhesion and friction dynamics of a railway vehicle. After the description of a nonlinear estimator model its observability is analyzed and the estimator set-up is discussed. The presented test rig results reveal a reliable and accurate performance of the estimator

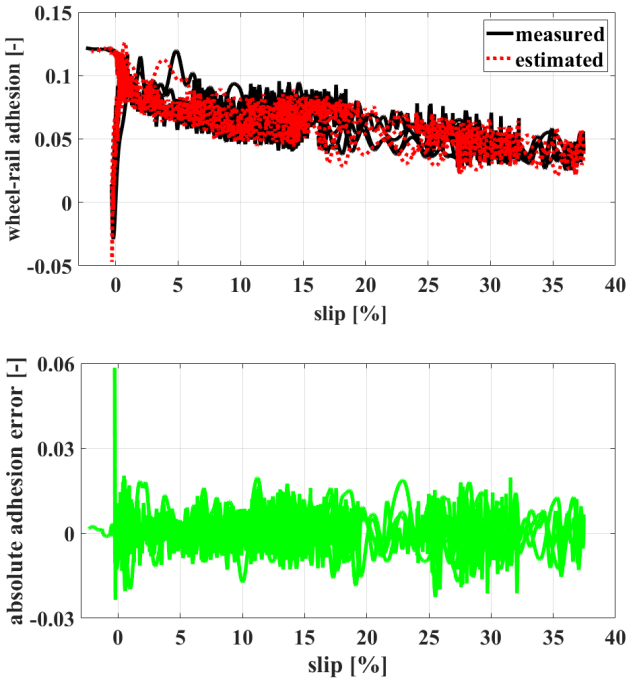

Fig. 6. Top: Comparison of adhesion-over-slip results in a sanding scenario; bottom: Absolute error between estimated and measured adhesion

in challenging scenarios with rough operating conditions. In the end, this work highlights the benefits of mechatronic components in railway systems and especially the potential of an estimator in terms of an advanced longitudinal dynamics control.

To bring this concept one step further towards the application in modern trains, there are some tasks to be tackled. First of all, the estimator has to be implemented on a real-time control unit what we will go about in the context of the upcoming test rig construction at our institute. Secondly, the new estimator set-up has to be closely examined during the operation of a train on a real track. Finally, the fields of application have to be demonstrated that allow for the exploitation of the adhesion and friction estimations. For the sake of an increased rail network capacity the adhesion estimation might be integrated into an improved and extended wheel-slide protection and anti-skid system, so that the required train distances can be reduced. Since this use case accounts for an expensive homologation process, another idea that might be easier to realize is to define a monitoring strategy for brake and traction components. The advantage of such a system is that there is no need for a new homologation process, since there is no direct feedback on the vehicle dynamic behavior.

ACKNOWLEDGEMENTS

The authors would like to thank Dr. Jonathan Brembeck for his valuable support in the estimator design. Furthermore, the authors would like to thank the colleagues of Knorr-Bremse Rail Vehicle Systems for providing the test data.

REFERENCES

Brembeck, J., Pfeiffer, A., Fleps-Dezasse, M., Otter, M., Wernersson, K., and Elmqvist, H. (2014). Nonlinear state estimation with an extended fmi 2.0 co-simulation interface. In *Proceedings of the 10th International Modelica Conference*, 53–62. Lund, Sweden.

Charles, G., Goodall, R.M., and Dixon, R. (2008). Model-based condition monitoring at the wheel-rail interface. *Vehicle System Dynamics*, 46(sup1), 415–430.

Gauthier, J.P., Hammouri, H., and Othman, S. (1992). A simple observer for nonlinear systems applications to bioreactors. *IEEE Transactions on Automatic Control*, 37(6), 875–880.

Hermann, R. and Krener, A. (1977). Nonlinear controllability and observability. *IEEE Transactions on Automatic Control*, 22(5), 728–740.

Ostermeyer, G. (2003). On the dynamics of the friction coefficient. *Wear*, 254(9), 852–858.

Polach, O. (2005). Creep forces in simulations of traction vehicles running on adhesion limit. *Wear*, 258(7), 992–1000.

Ricciardi, V., Augsburg, K., Gramstat, S., Schreiber, V., and Ivanov, V. (2017). Survey on modelling and techniques for friction estimation in automotive brakes. *Applied Sciences*, 7(9), 873.

Schindler, C. (ed.) (2014). *Handbuch Schienenfahrzeuge-Entwicklung, Produktion, Instandhaltung*. DVV Media Group GmbH, Hamburg.

Schwarz, C., Brembeck, J., and Heckmann, B. (2019a). Dynamics observer for the longitudinal behavior of a wheelset on a roller rig. *Proceedings of the Institution of Mechanical Engineers, Part F: Journal of Rail and Rapid Transit*, 233(10), 1112–1119.

Schwarz, C. and Keck, A. (2019). Observer synthesis for the adhesion estimation of a railway running gear. *IFAC PapersOnLine*, 52(15), 319–324.

Schwarz, C., Lüdicke, D., and Heckmann, B. (2019b). Friction estimation for railway brake systems in field tests. In *2nd International Railway Symposium Aachen*, 608–623. Aachen, Germany.

Shrestha, S., Wu, Q., and Spiryagin, M. (2019). Review of adhesion estimation approaches for rail vehicles. *International Journal of Rail Transportation*, 7(2), 79–102.

Simon, D. (ed.) (2006). *Optimal State Estimation: Kalman, H Infinity, and Nonlinear Approaches*. Wiley & Sons, 1st edition.

Strano, S. and Terzo, M. (2018). On the real-time estimation of the wheel-rail contact force by means of a new nonlinear estimator design model. *Mechanical Systems and Signal Processing*, 105, 391–403.

Umweltbundesamt (2019). Emissionsdaten. URL `https://www.umweltbundesamt.de/themen/verkehr-laerm/emissionsdaten#verkehrsmittelvergleich_personenverkehr`.

Ward, C.P., Goodall, R.M., Dixon, R., and Charles, G.A. (2012). Adhesion estimation at the wheel–rail interface using advanced model-based filtering. *Vehicle System Dynamics*, 50(21), 1797–1816.